HHS Public Access

Author manuscript

Radiat Res. Author manuscript; available in PMC 2025 January 01.

Published in final edited form as:

Radiat Res. 2024 January 01; 201(1): 35–47. doi:10.1667/RADE-23-00064.1.

Chemokine Receptor CXCR4 Radioligand Targeted Therapy Using ^{177}Lutetium-pentixather for Pulmonary Neuroendocrine Cancers

Melissa A. Fath[a,1,2], **Dijie Liu**[b,2], **Jordan T. Ewald**[a], **Claudia Robles-Planells**[b], **Ann M. Tomanek-Chalkley**[a], **Stephen A. Graves**[c], **James R. Howe**[d], **Thomas M. O'Dorisio**[e], **Prerna Rastogi**[f], **Andrew M. Bellizzi**[f,2], **M Sue O'Dorisio**[b,2], **Yusuf Menda**[c,2], **Douglas R. Spitz**[a,1,2]

[a]Free Radical and Radiation Biology Program, Department of Radiation Oncology, Holden Comprehensive Cancer Center, University of Iowa, Iowa City, Iowa 52240

[b]Department of Pediatrics, Holden Comprehensive Cancer Center, University of Iowa, Iowa City, Iowa 52240

[c]Department of Radiology, Holden Comprehensive Cancer Center, University of Iowa, Iowa City, Iowa 52240

[d]Department of Surgery, Holden Comprehensive Cancer Center, University of Iowa, Iowa City, Iowa 52240

[e]Department of Internal Medicine, Holden Comprehensive Cancer Center, University of Iowa, Iowa City, Iowa 52240

[f]Department of Pathology, Holden Comprehensive Cancer Center, University of Iowa, Iowa City, Iowa 52240

Abstract

Intermediate to high-grade lung neuroendocrine tumors (NETs; i.e., atypical carcinoid tumors) and neuroendocrine carcinomas (NECs) are currently difficult to cure. These tumors were found to express the CXCR4 G-protein coupled receptor that can be targeted with radioligands. PCR and flow cytometric analysis of lung NET and NEC cell lines using an anti-CXCR4 antibody demonstrated that all cell lines tested expressed CXCR4. PET/CT imaging with ^{68}Galium-pentixafor in mouse xenografts of NETs and NECs verified tumor targeting that was blocked by a CXCR4 agonist. Clonogenic survival analysis demonstrated a more than additive enhancement of killing when 1 μM auranofin (a thioredoxin reductase inhibitor) was used as a radiosensitizer in combination with ^{177}Lu-pentixather (10 μCi). DMS273 small cell lung cancer xenografts in female nude mice treated with 25 μCi/g ^{177}Lu-pentixather induced inhibition of tumor growth and resulted in an increase in overall survival without causing unacceptable normal tissue toxicities. Immunohistochemical staining of 95 retrospective human samples (containing 90 small cell lung carcinomas) demonstrated 84% CXCR4 positivity. In a multivariable analysis of this cohort that

[1]Corresponding authors: Melissa A. Fath, PhD, Associate Research Scientist, Adjunct Assistant Professor, melissa-fath@uiowa.edu; and Douglas R. Spitz, PhD, Professor and Director, douglas-spitz@uiowa.edu. Free Radical and Radiation Biology Program, Department of Radiation Oncology, Holden Comprehensive Cancer Center, University of Iowa, Iowa City, IA 52240.
[2]These authors contributed equally to the manuscript preparation.

included age, gender, stage, primary site, SSTR2 status, and CXCR4 status, Cox regression models determined that only distant metastasis at presentation ($P < 0.01$) and a CXCR4 H-score >30 ($P = 0.04$) were significantly associated with reduced survival. Prospective clinical testing of patient tumors identified CXCR4-positivity in 76% of 21 NECs, 67% of 15 lung NETs (including 8 of 10 atypical carcinoids), and 0% of 25 non-lung NETs (including 5 NETS G3s). These data support the hypothesis that CXCR4-targeted theranostics can be utilized effectively for select NETs and NECs.

INTRODUCTION

Atypical carcinoid tumors and neuroendocrine carcinomas (NECs) of lung origin currently have poor prognoses, with most patients dying within five years. A subset of pulmonary neuroendocrine tumors (NETs) may respond to radioligand therapy targeting somatostatin receptor subtype 2 (SSTR2), and NECs ([including small cell lung cancer (SCLC)] may initially respond to chemotherapy, though resistance to therapy inexorably occurs, leading to progression and death; this highlights a critical need for new therapeutic strategies (1, 2). The majority of these cancers express the G protein coupled receptor, C-X-C chemokine receptor 4 (CXCR4) as demonstrated by immunohistochemistry, making CXCR4 an attractive target for cancer diagnosis and treatment. CXCR4 can be targeted with pentixather and/or pentixafor that can be radiolabeled for both imaging and therapy. Ga-pentixafor and Lu-pentixather exhibit high affinity for human CXCR4 with IC50s of 24.8 ± 2.5 nM and 14.6 ± 1.0 nM, respectively (3). Pentixather also shows enhanced lipophilicity, relative to Ga-pentixafor, as well as excellent in vivo stability. As opposed to non-radioactive CXCR4-targeted approaches, the efficacy of pentixather labeled with ^{177}Lutetium exhibits crossfire or bystander effects from CXCR4-positive cells to adjacent potentially receptor-negative tumor cells (4). A recent study of the pharmacokinetic profile of ^{177}Lu-pentixather demonstrated excellent in vivo CXCR4-targeting with high tumor uptake and retention, leading to high radiation doses to tumor tissue during targeted radioligand therapy (RLT). These data support the potential of ^{68}Ga-pentixafor/^{177}Lu-pentixather in CXCR4-targeted theranostics (5).

Currently there are phase 1 clinical trials testing CXCR4 targeted radionuclides for cancer diagnosis and therapy in hematologic malignancies using ^{177}Lu-pentixather (6). Furthermore ^{68}Ga-pentixafor targeting CXCR4 is used for diagnosis of hematologic malignancies (7, 8). A recent study evaluating ^{68}Ga-pentixafor PET on 690 patients with different cancer types including 12 SCLC patients found high tumor uptake and tumor-to-background contrast compared to ^{18}Fluoro-deoxyglucose-PET (9).

In the current study, we investigate CXCR4 expression in human pulmonary neuroendocrine neoplasms using both tumor cell lines and human lung biopsies. We confirm the specificity of ^{68}Ga-pentixafor as a PET imaging agent pre-clinically with atypical carcinoid and neuroendocrine carcinoma. We also evaluate, for the first time in vitro and in vivo, the therapeutic potential of ^{177}Lu-pentixather to specifically target CXCR4 for improving therapy responses in SCLC and drug-resistant SCLC in preclinical models.

MATERIALS AND METHODS

Cell and Culture Conditions

Neuroendocrine tumor and carcinoma cell lines (including DMS53, H209, H69, H69AR, H727 and H720) and H292 cancer cell lines were obtained from American Type Culture Collection (ATCC) and DMS 273 cells from ECSCC through Sigma-Aldrich. H720 cells were maintained in DMEM/F12 medium supplemented with 5% fetal bovine serum (FBS) and other ingredients according to ATCC recommendations, with all other cells maintained in RPMI1640 medium supplemented with 10% FBS (Hyclone) and penicillin-streptomycin (Gibco) or 0.01% gentamycin sulfate (Cellgro). All cells were maintained at 37°C with 5% CO_2 and have been authenticated by evaluating their Human 9-marker STR profile (IDEXX BioAnalytics, Columbia MO).

Mice

All animal experiments were conducted in compliance with protocols approved by the Animal Care and Use Committee of the University of Iowa. The mice were housed in a temperature- and humidity-controlled room with a 12/12-h light/dark schedule. Mice were fed clean rodent chow and water ad libitum. Four- to six-week-old female SHO (SCID hairless outbred) mice were purchased from Charles River Laboratories for imaging studies. Four- to six-week-old female athymic nu/nu mice were purchased from Envigo for the therapy study.

Quantitative PCR RNA Isolation, qPCR and GPCR Array Expression

Total RNA was extracted from cultured cells, or freshly frozen primary tumors and adjacent normal tissue using TRIzol reagent (Life Technology), and 2 μg of total RNA was converted to cDNA using the High Capacity cDNA Reverse Transcription Kit according to manufacturer's instructions (Applied Biosystems). cDNA was assayed using the Taqman human GPCR Array kit (Applied Biosystems, 367 GPCR and 14 control genes) with a ABI 7900 HT Fast RT-PCR System. Data was analyzed using SDA v2.3 software with manual CT set to 0.2, and individual CT values reviewed for each gene. Results for cell lines, human tissues and tumors were analyzed by comparative CT method using Data Assist Software with a two-sample, two-tailed Student's t-test; p values were adjusted using Benjamin-Hochberg False Discovery Rate. cDNA from cells were tested with TaqMan Gene Expression Assay probes (Applied Biosystems HS00607 for CXCR4, HS027866224-g1 for GAPDH or 18S) for qPCR assay. ΔCT was calculated by subtracting the CT of a GAPDH the internal control gene. The gene expression level for H292 cells was set as 1; other cells were normalized accordingly by comparing the ΔΔCT and the fold-change was presented for mRNA expression for each gene. Three experiments were performed for each sample in duplicates and the results were averaged.

Flow Cytometry

Cells were harvested after incubation with enzyme-free cell dissociation solution (Millipore Inc). One million cells/in 30 μl binding buffer (0.2% BSA in PBS) were incubated with APC-conjugated anti-human CXCR4 monoclonal IgG2A antibody (BioLegend, Inc.) or

isotype antibodies (BioLegend, Inc.) on ice for 30 min in the dark. After incubation, cells were rinsed twice with ice-cold binding buffer, resuspended in 0.5 ml binding buffer and filtered through a 70-μm nylon cell strainer prior to analysis on a Beckmann Dickinson LSR-Violet Flow Cytometer. The Hoechst channel was used for cell viability monitoring. UltraComp beads (Life Technology) were used for compensation. The tests were performed 3 times, and the data was analyzed by FlowJo software.

Radiolabeling Pentixafor with $^{68}GaCl_3$ and Pentixather with $^{177}LuCl_3$

$^{68}GaCl_3$ was eluted from a $^{68}Ge/^{68}Ga$ generator with 10 ml 0.1 M HCl through a SXC column (Strata X polymeric strong cation column, 33 μm, 30 mg/ml, Phenomenex) and using 0.25 ml N2 Solution (0.5% concentrated HCl/1.5% H2O in acetone) followed by 0.2 ml acetone. Twenty micrograms of pentixafor (PentixaPharm®, Germany, reconstituted in metal-free H_2O) was labeled with ~3–4 μCi (111–148 MBq) of ^{68}Ga in 0.5 ml 0.4 M sodium acetate buffer (pH 5.3–5.5) at 95°C for 15 min. The reaction mixture was purified using a SC column (Strata X column, polymeric reversed phase, 33 μm, 30 mg/ml, Phenomenex). ^{68}Ga-pentixafor was eluted in 0.3 ml 50% ethanol-saline solution and further diluted in saline to decrease the ethanol concentration to less than 10% before injection to the mice as a PET imaging radiotracer. The peptide pentixather acetate was received from ABX (Lot no. 20191001) and reconstituted in water to a concentration of 1 μg/μl and stored at −20°C. Non-carrier ^{177}lutetium was received from Isotope Technologies Garching GmbH (Germany). Pentixather as a 1 μg/μl concentration in 300 μl of ascorbic acid buffer (50 mg/ml from Polatom, Poland) (pH 4) was mixed with $^{177}LuCl_3$ (at approximately ratio of 1 μg per 37 MBq of ^{177}Lutetium) at 95°C for 27 min with shaking (450 rpm). The reaction mixture was purified as described above and eluted in 0.3 ml 50% ethanol in saline containing ascorbate buffer (1 mg/ml). The eluent was further diluted in normal saline for the SPECT imaging and therapy study.

Clonogenic Survival Analysis

DMS273, DMS53 or H69AR cells (240,000/60 mm dish) were plated and allowed to grow in tissue culture media for 24 h. Cells were then treated with AMD3100 (Plerixafor, a CXCR4 antagonist) for 5 min before and during treatment with 10 μCi ^{177}Lu-pentixather and/or auranofin 1 μM for 3 h, after which clonogenic survival was measured as described here: Floating cells in medium were collected and combined with the attached cells from the same dish that were trypsinized with 1 mL trypsin-EDTA (CellGro). Samples were centrifuged, and cells were counted with a Beckman Coulter counter. Cells were plated at low density (150–150,000 cells per dish), and clones were allowed to grow for 14 days in maintenance media containing 0.1% gentamycin. Cells were then fixed with 70% ethanol and stained with Coomassie blue for analysis of clonogenic survival. Individual assay colony counts were normalized to that of control of the same cell line, with at least 3 cloning dishes per condition repeated in at least 2–3 separate experiments.

Micro-PET/CT and Micro-SPECT/CT Imaging and Biodistribution in Mice Bearing SCLC Xenografts

Three to four weeks after subcutaneous implantation (at the shoulder or flank) of SCLC cells, when the tumor size reached 150–500 mm^3, mice were administered ^{68}Ga-pentixafor

via tail vein injection (approximately 11.1 MBq). Mice were imaged 1 h after injection using a micro-PET/CT imaging instrument (Siemons Inveon, at the Small Animal Imaging Core, University of Iowa) for 30 min followed by a 15 min CT scan. At the end of imaging, mice were euthanized promptly (approximately 1.75 h after injection). Major organs, tissues and tumors were dissected, weighed, and counted using a Packard Cobra II Auto-Gamma Counter and the radioactivity was presented as the percentage of injected dose per gram of tissues (% ID/g) with decay correction.

Two mice bearing right flank DMS273 tumor xenografts were also administered ^{177}Lu-pentixather (approximately 15.6 MBq) via tail vein injection for sequential micro-SPECT imaging to monitor the biodistribution profile. Mice were imaged at 4, 24 and 96 h after injection using a micro-SPECT/CT imaging instrument (Siemons Inveon) followed by a biodistribution study as described above.

CXCR4 Immunohistochemistry and Tissue Microarray (TMA) Construction

CXCR4 immunohistochemistry was performed on 4-lm-thick tissue sections after PT Link (Agilent Dako; Santa Clara, CA) deparaffinization, rehydration, and heat-induced epitope retrieval in HpH Target Retrieval Solution (Agilent Dako; pH 9) on an Autostainer Link 48 (Agilent Dako) using a rabbit monoclonal antibody (clone UMB2; Abcam; Cambridge, MA; 1:250 dilution; 15 min incubation) and the polymer-based EnVision FLEX detection system (Agilent Dako; 15 min incubation). A multi-tissue block served as the positive control with expected strong and moderately strong staining in germinal center cells and mantle zones in the tonsil and negative staining in tonsillar epithelium, myometrium, normal colon, normal lung tissue, and placenta. CXCR4 expression was assessed for extent (0–100% of cells staining) and intensity (0–3+) to calculate an H-score ranging from 0–300 for each tissue. Tissue microarrays were constructed from samples of small cell carcinoma (of pulmonary and extrapulmonary visceral origin), Merkel cell carcinoma, and ileal and pancreatic NETs identified in the tissue archives of the University of Iowa Hospitals and Clinics from 1983 to 2013. The same CXCR4 assay was used to stain the TMAs and in prospective clinical testing. The UMB2 rabbit monoclonal antibody was selected for assay development, as multiple widely used monoclonal (e.g., 12G5, 44716) and polyclonal CXCR4 antibodies have been shown to lack specificity to the linear epitopes detected by IHC (10).

^{177}Lu-pentixather Efficacy Study in Tumor-bearing Mice

For the efficacy study, 1×10^6 DMS273 cells were implanted subcutaneously into the right flanks of nude mice and grew for 7 days, with tumor volume approximately 30 mm^3, estimated by Vernier calipers [volume = (length × width^2)/2]. Animals were randomized into treatment and control groups (n = 9 per group). Mice were administered 300 μl saline/arginine/lysine intraperitoneally 30 min before and 1 h after IV injection of ^{177}Lu-pentixather (25 μCi/g). To prepare the lysine/arginine solution, 375 mg L-lysine USP and 375 mg L-arginine USP (Dot Scientific) were dissolved in 4.3 ml of 0.9% NaCl and diluted with 25 ml sterile water. The solution was adjusted to a neutral pH using HCl; final volume was adjusted to 30 ml with water and filtered into a sterile vial. Mice were monitored, weighed and tumor volume measured daily with Vernier calipers. Animals were euthanized when tumor length exceeded 1500 mm for two days. On Day 13 post-treatment,

blood was obtained via tail vein and diluted 1:10 in PBS and a complete blood cell count (CBC) processed in a Siemens ADVIA 120 Hematology Analyzer. At euthanasia, blood was obtained via cardiac puncture and serum chemistry was analyzed to evaluate liver and renal functionality (by Antech Diagnostic). Kidneys, liver, and femurs were collected for toxicity evaluations.

Bone Marrow Harvest and Flow Cytometry

Whole bone marrow cells were obtained by flushing one femur with PBS containing 2% FBS followed by erythrocyte elimination with ACK Lysing Buffer (10–548E, BioWhittaker, Lonza). The remaining cells were filtered through a 40-lm pore size cell strainer and counted. One million cells were stained with Zombie Aqua (423102, BioLegend) for 20 min at room temperature for live/dead cell discrimination, followed by a 30 min surface staining on ice using PBS with 1% BSA as staining buffer with allophycocyanin (APC)-conjugated, lineage negative (Lin-) cocktail (BD Bioscience), PerCP/Cy5.5-conjugated anti-Sca1 (Clone D7, BioLegend), APC/Cy7-conjugated anti-cKit (Clone 2B8, BioLegend), PE-conjugated anti-CD135 (Clone A2F10, BioLegend), FITC-conjugated anti-CD48 (Clone HM48–1, BioLegend), PE/Cy7-conjugated anti-CD150 (Clone TC15-12F12.2, BioLegend) and BV421-conjugated anti-CXCR4 (Clone L276F12, BioLegend). Cells were immediately analyzed using an LSR II flow cytometer (Becton Dickinson). The analysis of Lin-, LSK (Lin- cKit+ Sca1+), MPP2 (Erythrocyte/platelet multipotential progenitor subset 2) (Lin- cKit+ Sca1+ CD135- CD48+ CD150+), MPP3 (Granulocyte/Monocyte multipotential progenitor subset 3) (Lin- cKit+ Sca1+ CD135- CD48+ CD150-), MPP4 (Lymphoid primed progenitor subset 4) (Lin- cKit+ Sca1+ CD135+ CD150-), ST-HSC (short term hematopoietic stem cell) (Lin- cKit+ Sca1+ CD135- CD48- CD150-), and LT-HSC (long term hematopoietic stem cell) (Lin- cKit+ Sca1+ CD135- CD48+CD150-) populations was performed using FlowJo Software (Treestar).

Statistical Analysis

The analysis of the in vitro data was performed using two-way ANOVA uncorrected Fisher's LSD on Graph Pad Prism software. The analysis of in vivo results focused on treatment group comparisons of tumor growth and survival. Given the initial delay in tumor growth, non-linear mixed effects regression models were used to estimate and compare tumor growth curves using SAS v9.4 (SAS Institute, Cary, NC). Random effects were included to account for the longitudinally correlated nature of repeat tumor measurements within a mouse. Estimates of survival were obtained with the Kaplan-Meier method and compared using log-rank tests.

Kidney and Liver Histology

After euthanasia, the kidney and the left lobe of the liver were fixed in 10% neutral buffered formalin and then paraffin embedded (FFPE). Each tissue was cut at 3 μm thickness using a Microm HM355 microtome. Kidneys were stained with H&E and PAS while livers were stained with H&E, PAS, and Masson's Trichrome. All staining was performed using a DRS-601 Autostainer with slides mounted for pathological analysis. Kidney tubular injury was assessed as vacuolization, loss of epithelial cell nuclei, dark acidophilic cytoplasm, loss of tubular epithelial cells into tubular lumen, and acellular sections of tubules. Livers were

assessed for fibrosis, necrosis, inflammation, mitotic activity, and hepatocyte cytoplasmic quality.

RESULTS

Lung Carcinoid and SCLC Cell Lines Express CXCR4 and ^{177}Lu-pentixather Induces CXCR4-dependent Clonogenic Cell Death

Quantitative RT-PCR was used to establish the mRNA expression level of CXCR4 compared to the human lung mucoepidermoid cell line H292, which was used as a negative control. Both typical and atypical lung carcinoid cell lines expressed CXCR4 (Table 1). All SCLC cell lines showed increased levels of immunoreactive CXCR4 on the cell surface after flow cytometric analysis, ranging from a fivefold increase in DMS53, to a 45-fold increase in DMS273, and a 85-fold increase in the multi-drug resistant cell line H69AR, that was selected using Adriamycin (11). These data continue to suggest that CXCR4 is a robust and significant potential target for the development of RLT in pulmonary NETs and NECs (SCLC) (Table 1).

Importantly, when DMS53, DMS273 and H69AR cells were treated in vitro with 10 μCi ^{177}Lu-pentixather, they exhibited cell death in proportion to CXCR4 expression (Fig. 1A). Furthermore, CXCR4-dependent clonongenic cell killing was confirmed by the ability of AMD3100, a selective CXCR4 antagonist, to nearly total inhibit the in vitro cytotoxicity of ^{177}Lu-pentixather (Fig. 1A). Finally, combination of ^{177}Lu-pentixather with the known radiosensitizer auranofin (12, 13), which inhibits thioredoxin reductase activity, resulted in significant enhancement of anti-tumor activity (Fig. 1B). These results clearly demonstrate that ^{177}Lu-pentixather selectively targets SCLCs expressing CXCR4, causing clonogenic cell killing that can be enhanced by a known radiosensitizing agent.

PET/CT Imaging Using ^{68}Ga-pentixafor Demonstrates Specific Tumor Targeting in Mice Bearing Xenografts

Pulmonary carcinoid and SCLC xenografts were generated on the shoulders of nude mice. When tumor size reached approximately 150–500 mm^3, 168–334 μCi ^{68}Ga-pentixafor was administered via tail vein followed by micro-PET/CT imaging 60 min later. The high pixel count in kidneys and bladders indicate the urinary tract as the primary route of ^{68}Ga-pentixafor excretion (Fig. 2). More importantly, as seen in Fig. 2A–C, ^{68}Ga-pentixafor identified all SCLC xenografts and demonstrated high tumor-to-background ratio in contrast to the lung mucoepidermoid cancer cell line H292, used as the negative control. Co-treatment with the CXCR4 antagonist AMD3100, and ^{68}Ga-pentixafor injection, significantly blocked ^{68}Ga-pentixafor accumulation in the tumors, again indicating the specificity of pentixafor binding to CXCR4 (Fig. 2D). Mice were euthanized 45 min after the images were obtained for Fig. 2A; tumors and organs were harvested for biodistribution studies as shown in Fig. 2E. DMS273 tumor uptake was significantly greater than in the H292 negative control.

Micro PET/CT using ^{68}Ga-pentixafor was also used to image mice bearing lung carcinoids H727 and H720 (Fig. 3A and B). Biodistribution performed 1 h after imaging demonstrated

radioligand accumulation in the tumors as well as accumulation in the lungs, kidneys and livers, indicating potential areas of toxicity with CXCR4 targeted therapy (Fig. 3C). These data support the conclusion of Lapa et al. (14) that non-invasive PET imaging with ^{68}Ga-pentixafor may be used as a diagnostic probe for CXCR4 expression in lung carcinoids and SCLCs.

^{177}Lu-pentixather SPECT Imaging and Biodistribution Demonstrate Accumulation in Tumor and Liver

While ^{68}Ga-pentixafor is an excellent PET imaging agent for diagnosis, ^{177}Lu-pentixather can be imaged with single photon emission tomography (SPECT), enabling accurate dosimetry calculations. Sequential SPECT imaging followed by biodistribution studies was performed in mice bearing DMS273 flank tumors. The mice were injected intravenously with ≈420 μCi of ^{177}Lu-pentixather and images were performed after 4, 24 and 96 h post-injection followed by euthanasia at 100 h post-injection; radioactivity of the organs of interest was measured using a c-counter with decay correction (Fig. 4A–C). ^{177}Lu-pentixather activity was rapidly cleared from stomach, intestines, and kidneys; hepatic activity levels remained persistently high up to 4 days post-injection. Biodistribution studies demonstrated an ~6% ID/g accumulation of the radiolabel in the liver at 100 h post-injection, suggesting slow hepatic clearance and continuous hepatobiliary excretion of the tracer.

^{177}Lu-pentixather Significantly Decreases SCLC Growth Rate and Prolongs Survival

Athymic nude mice (9 per group) bearing a right flank DMS273 tumor xenograft (7 days after implantation. approximately 3 mm in diameter) were injected with 25 μCi/g ^{177}Lu-pentixather or saline vehicle via tail vein. Thirty min before and 1 h after the ^{177}Lu-pentixather or saline injection, mice were treated with an intraperitoneal injection of a mixture of positively charged amino acids (arginine and lysine) to decrease renal uptake of ^{177}Lu-pentixather. A significant decrease in average tumor growth rate was observed with ^{177}Lu-pentixather treatment compared to control ($P = 0.04$, Fig. 5A). Mice treated with ^{177}Lu-pentixather showed a significantly increased median overall survival compared to control, 26 days vs. 17 days ($P = 0.012$, Fig. 5B). Individual tumor growth and tumor weight values are shown in Supplementary Fig. S1[3] (https://doi.org/10.1667/RADE-23-00064.1.S1). There was no significant change in body weight in any mice in either control or treatment groups (Fig. 5C) and all mice maintained a body condition score of 3 indicating general good health (15).

Evaluation of Potential Therapy-limiting Toxicity

Whole blood was drawn from each mouse and a complete blood count (CBC) was performed on day 13 after treatment with ^{177}Lu-pentixather (Fig. 6). Mice in the treatment group had significantly fewer platelets vs. control mice ($923 \times 10^3/\mu l \pm 143$ vs. $1319 \times 10^3/\mu l \pm 83$ $P < 0.001$). An additional CBC, performed at the time of euthanasia, 19–37 days after ^{177}Lu-Pentixather treatment, demonstrated no further change in platelet count of the

[3]Editor's note. The online version of this article (DOI: https://doi.org/10.1667/RADE-23-00064.1) contains supplementary information that is available to all authorized users.

treated mice ($878 \times 10^3/\mu l \pm 159$) indicating neither a recovery nor worsening of toxicity. There were no deficiencies in red blood cell parameters in treated vs control mice; however, there was a slight but significant decrease in white blood cells, mainly due to the highly significant decrease in neutrophils, which had recovered by the time of euthanasia (27 ± 17.5% vs. 27 ± 9.5% SD) in treated vs. control animals.

Bone marrow cells (red blood cells removed) were harvested from mice femurs at euthanasia and stained for hematopoietic stem and progenitor cell (HSPC) markers to examine long-term hematologic toxicity using flow cytometry. Because CXCR4 is expressed on both human and mouse bone marrow HSPCs (16, 17), they are considered a secondary cell target when CXCR4 RLT is used. There was no decrease in the bone marrow CXCR4+ cells (Supplemental Fig. S2; https://doi.org/10.1667/RADE-23-00064.1.S1), which supports the low selectivity of murine CXCR4 (mCXCR4) compared to human CXCR4 (18) to ^{177}Lu-pentixather. In this context, the significant decrease observed in the long-term hematopoietic stem cell (LT-HSC) population after ^{177}Lu-pentixather treatment (Fig. 7) suggests an indirect long-term bone marrow toxicity, while other stem and progenitor populations remained stable as compared to the control mice.

Furthermore, blood drawn at euthanasia was also evaluated for clinical chemistry markers of liver and kidney function (Fig. 8). There were no significant differences between treated and untreated groups, indicating no acute toxicities from 25 μCi of ^{177}Lu-pentixather.

Because sequential SPECT imaging demonstrated extended ^{177}Lu-pentixather retention in the liver (Fig. 4), a blinded review of liver histology was performed after euthanasia by a pathologist. The trichrome stains demonstrated no fibrosis and PAS-D stains demonstrated no debris in any of the specimens. The H&E-stained slides were assessed for readily identifiable mitotic activity, rarefied hepatocyte cytoplasm, and hepatitis. Mitotic activity was found in 4 out of 9 treated livers and 7 out of 9 control livers, indicating no differences caused by ^{177}Lu-pentixather treatment. Hepatocellular injury manifested as “rarefied” hepatocyte cytoplasm due to clumping of organelles, was found in 4 out of 9 livers and 5 out of 9 control livers after ^{177}Lu-Pentixather treatment, again showing no significant differences (data not shown).

Because of the significant renal uptake and primary renal excretion of ^{177}Lu-pentixather, kidneys were also evaluated by a pathologist for tubular injury, tubulointerstitial inflammation, glomerular changes, and interstitial fibrosis. Inflammation, glomerular changes, and interstitial fibrosis were absent in all samples. Tubular injury was defined as stained bodies of various sizes, vacuolization, loss of epithelial cell nuclei, dark acidophilic cytoplasm, loss of tubular epithelial cells into the tubular lumen, and acellular tubular sections and toxicity assessed on a scale of 1 (mild) to 4 (severe). There were no injuries ranked 4 in either treated or control groups. One mouse ranked 3 in tubular injury in both control and ^{177}Lu-pentixather treatment groups. There were two vs three mice ranked 2 in tubular injury in control vs treatment (Fig. 9A). QPCR was performed for KIM1and NGAL, two molecular markers of early kidney damage; there was no significant difference in injury between treatment and control groups (Fig. 9B and C).

Most Human NECs Express CXCR4 That Positively Correlates with Poor Prognosis

In a retrospective TMA cohort, 84% of 95 NECs, including 94% of 31 SCLCs, 76% of 21 extrapulmonary visceral small cell carcinomas, and 81% of 43 Merkel cell carcinomas were positive as indicated by CXCR4 immunohistochemistry (IHC) (Fig. 10 and Table 2). The median H-score for positive tumors was 120. Eleven percent of 28 pancreatic NETs showed positivity in rare cells (median H-score only 3), while 38 ileal NETs were uniformly negative. In a multivariate analysis including age, gender, stage at diagnosis (localized, regional, distant), primary site (lung, extrapulmonary viscera, skin), and SSTR2 IHC, only the presence of distant metastasis at presentation (HR 4.02, 95% CI 1.88–8.60; $P < 0.01$) and a CXCR4 H-score >30 (HR 2.50; 1.05–5.98; $P = 0.04$) significantly predicted lower overall survival. In prospective clinical IHC testing, CXCR4-positivity was found in 76% of 21 NECs (mean; median H-score 181; 255) and 0% of 25 non-pulmonary NETs (including 5 G3 NETs). Sixty-seven percent of 15 lung NETs, including 8 of 10 atypical carcinoid tumors, were CXCR4-positive (mean; median H-score 102; 130 for atypical carcinoid tumors).

DISCUSSION

Lung neuroendocrine neoplasms include typical carcinoid tumors, atypical carcinoid tumors, and small and large NECs. While most typical carcinoid tumors are resected and are associated with favorable prognosis (i.e., a 5-year survival rate exceeding 80%), atypical carcinoid tumors are frequently aggressive (5-year survival around 50%), while small and large cell NEC are among the most aggressive malignancies with 5-year survival in stage IV disease less than 5% (19). Typical and atypical carcinoid tumors roughly correspond to the G1 and G2 grades used in the classification of gastroenteropancreatic NETs, though atypical carcinoid tumors with Ki-67 proliferation indices exceeding 20% (i.e., G3 range) are increasingly recognized, in particular at metastatic sites (20, 21). Due to occasional high expression of SSTR2 in typical pulmonary carcinoids, somatostatin analogue therapy targeting SSTR2 with ^{177}Lu-DOTATATE has improved outcomes for patients with typical carcinoids and is a mainstay of treatment. However, SSTR2 targeted RLT efficacy in atypical carcinoids and NECs is controversial (22, 23). Atypical carcinoids of the lung are currently considered incurable, with most patients succumbing to disease within five years. For SCLC, which accounts for 15% of bronchogenic carcinomas, combination treatment with platinum compounds and etoposide is the most widely-used therapy and can enhance survival, but this regimen is rarely curative and the average survival time for patients with SCLC is 10 months, with a 2-year survival rate of only 6% (23, 24). More recent clinical trials have demonstrated an enhanced overall survival and progression-free survival combining immune checkpoint inhibitors with chemotherapy; however, mixed results have been reported and the cost-effectiveness of these treatments are in question (25). There is a critical need to develop novel approaches for high-grade NETs and NECs.

CXCR4 is a G-protein-coupled receptor specific for cytokine CXCL12 (also known as stromal-derived-factor-1). In normal tissues, CXCR4/CXCL12 interactions induce hematopoietic stem cell migration and differentiation, B-cell proliferation and T-cell recruitment, thereby providing immunosurveillance (26). Within the context of cancer,

CXCL12/CXCR4 activation supports a variety of tumor-growth functions including proliferation, angiogenesis and stimulation of migration of CXCR4-expressing cells to tissues with high CXCL12 expression (liver, bone marrow, lung, lymph nodes) (27–29). Importantly, pathological CXCR4 expression has been documented in multiple human malignancies, including prostate cancer, breast cancer, lymphoma, leukemia, and melanoma (30). Using both human cancer cell lines and clinical data, we observed that 70–80% of these high-grade pulmonary malignancies express moderate to high levels of CXCR4. Likewise, Kaemmerer et al. found high intensity IHC staining of CXCR4 in almost all of 34 SCLC patient samples and varied expression levels in 30 atypical lung carcinoids (31).

Various anticancer drugs that target the CXCR4/CXCL12 axis are being investigated in humans. Plerixafor (AMD3100; Mozobil) is an immunostimulant that is FDA-approved for use in hematopoietic stem cell mobilization and harvest prior to autologous transplant. Likewise, the inhibitor Motrixafartide (BL-8040) showed highly significant and clinically meaningful results supporting its use in combination with granulocyte colony stimulating factor (GCSF) for mobilization of hematopoietic stem cells for subsequent harvest and transplantation in patients with multiple myeloma (32). Another CXCR4 antagonist, Mavorixafor (X4P-001), was shown to enhance infiltration of CD8+T cells and activation of the tumor microenvironment in melanoma patients (33). However, a randomized clinical trial evaluating a CXCR4 peptide antagonist LY2624587, as add on therapy for extensive disease SCLC (NCT01439568) was not efficacious using a 20 mg dose delivered subcutaneously (34).

Targeting CXCR4 in tumors with ^{68}Ga-pentixafor for PET/CT imaging has been widely investigated in hematological malignancies (Clinic trials: NCT05255926, NCT05093335, NCT04561492) and some solid tumors including SCLC patients. Buck et al. demonstrated a standardized uptake value (SUV) max of 12 and an average tumor-to-blood ratio of 7 in 12 SCLC patients with ^{68}Ga-pentixafor PET/CT, concluding these patients may benefit from CXCR4-targeted therapies (9). We used ^{68}Ga-pentixafor PET/CT to successfully visualize multiple SCLC and pulmonary NETs cell line xenografts in mouse models, with specific tumor uptake via CXCR4-mediated binding by co-injection of excess mass of pentixafor, while H292 xenograft showed negative tumor uptake which matched the in vitro Q-PCR and flow cytometry data as negative expression of CXCR4.

In addition, we used ^{177}Lu-pentixather sequential SPECT imaging followed by biodistribution studies to examine more closely the distribution of the therapeutic radioligand. ^{177}Lutetium emits β^- particles and low-energy gamma photons (35). The β^- particles are cytotoxic, inducing single stranded DNA breaks and generating reactive oxygen species while the low-energy gamma photons enable SPECT imaging with serial imaging being used for dosimetry calculations. Previous preclinical studies have demonstrated delayed whole-body clearance of ^{177}Lu-pentixather and high tumor accumulation in a xenograft model of B-cell lymphoma. Tumor/background ratios at 7 days after injection were 499 ± 202, 33 ± 7, 4.0 ± 0.8 and 116 ± 22 for blood, intestine, kidney and muscle, respectively (5). Further studies in a patient with multiple myeloma confirmed high tumor/kidney and tumor/liver dose ratios of 3.1 and 6.4 after a 7.8 GBq dose of ^{177}Lu-pentixather, with the kidneys being the dose-limiting organ (5, 36). Our SPECT

imaging data demonstrating accumulation of ^{177}Lu-pentixather in the liver 4 days after injection supports the data of Schottelius et al., who found hepatic ^{177}Lu-pentixather levels remained high up to 7 days after -injection, suggesting retention in the liver rather than slow and continuous hepatobiliary excretion of the tracer. However, co-injection of unlabeled AMD3100 partially blocked hepatic ^{177}Lu-pentixather uptake, suggesting a component of CXCR4-mediated liver accumulation (5).

Treatment of mice with 25 μCi/g ^{177}Lu-pentixather resulted in a decrease of neutrophils after two weeks, the expected nadir in mice after therapy, which is the first sign of bone marrow toxicity. Platelets showed a significant decrease after ^{177}Lu-pentixather treatment. There was a slight increase in lymphocytes after treatment, possibly due to the mobilization of these cells out of the bone marrow, as B-cells (lymphocyte subset) highly express CXCR4. Another subset of lymphocytes, T-cells, also express CXCR4; however, nude mice have greatly reduced T-cell numbers so these were not measured (37). With the time of blood draws of the ^{177}Lu-treated mice being between 20 and 30 days, this may align with the H2 classification of hematopoietic injury according to METREPOL (38). This classification falls under the umbrella of reparable hematopoietic injury if H2 classification is correct, indicating that the changes in blood parameters may not be permanent. These findings in the hematopoietic system underline the need for constant CBC measuring in future studies to understand the potential interaction between CXCR4 targeting molecules, radiation, and the blood. However, it has been demonstrated that most of the LT-HSC population is dispensable for steady-state hematopoiesis, and blood cell generation can be maintained by progenitor cells with minimal input from residual HSCs (39, 40). Limited clinical experience in patients with hematological malignancies and solid tumors with ^{177}Lu-pentixather indicate that due to significant bone marrow accumulation, treatments may need to be planned as myeloablative therapies supported by stem cell transplantation (9).

As the liver and kidneys demonstrate high levels of uptake of ^{177}Lu-pentixather, these also need to be considered for potential toxicity. Because RLT are primarily cleared thorough renal glomerular filtration with reabsorption/retainment at the proximal tubules exposing the kidneys to additional radiation, the kidneys have previously been reported as a dose-limiting organ for ^{177}Lu-based radiolabeled peptides. Many dosing regimens are designed around preventing renal absorbed doses (41). As was performed in our pre-clinical studies, a cocktail of lysine and arginine can be administered before and after injection of the radioactive peptide ligand to increase the rate of excretion, thereby protecting the kidneys, which are the dose-limiting organ in RLT. CXCR4 is reportedly constitutively expressed in the livers of mice (36) and in human hepatocytes close to the central vein (42), When assessed by histopathology, both liver and kidneys demonstrate no significant injury in the treatment group compared to controls. The lack of liver injury after histology, despite prolonged retention of ^{177}Lu-pentixather, is corroborated by nonsignificant changes in serum total bilirubin and alanine transaminase. Similarly, serum calcium and creatinine were within normal ranges for treated mice, supporting the absence of renal damage observed by pathological examination.

Taken together, our preclinical data highlights CXCR4 as a clinical target and demonstrate the efficacy of ^{68}Ga-pentixafor and ^{177}Lu-pentixather as complementary diagnostic and therapeutic agents in the currently difficult-to-cure malignancies, lung NETs and NECs.

Supplementary Material

Refer to Web version on PubMed Central for supplementary material.

ACKNOWLEDGMENTS

The authors would like to thank Gareth Smith for graphical assistance, the HCCC Biostatics Core for assistance with statistical analysis of animal experiments, and the Small Animal Imaging Core (SAIC), and Flow Cytometry Core at the University of Iowa for technical assistance. These studies were supported by NIH grants P50 CA174521, R01 CA243014, R50 CA243693, P01 CA217797, and P30 CA086862.

REFERENCES

1. Herzog BH, Devarakonda S, Govindan R. Overcoming Chemotherapy Resistance in SCLC. J Thorac Oncol 2021; 16(12): 2002–15. [PubMed: 34358725]
2. Naraev BG, Ramirez RA, Kendi AT, Halfdanarson TR. Peptide Receptor Radionuclide Therapy for Patients with Advanced Lung Carcinoids. Clin Lung Cancer 2019; 20(3):e376–e92. [PubMed: 30910575]
3. Osl T, Schmidt A, Schwaiger M, Schottelius M, Wester HJ. A new class of PentixaFor- and PentixaTher-based theranostic agents with enhanced CXCR4-targeting efficiency. Theranostics 2020; 10(18):8264–80. [PubMed: 32724470]
4. Brady D, O'Sullivan JM, Prise KM. What is the Role of the Bystander Response in Radionuclide Therapies? Front Oncol 2013; 3:215. [PubMed: 23967404]
5. Schottelius M, Osl T, Poschenrieder A, Hoffmann F, Beykan S, Hanscheid H, et al. [(177)Lu]pentixather: Comprehensive Preclinical Characterization of a First CXCR4-directed Endoradiothera-peutic Agent. Theranostics 2017; 7(9):2350–62. [PubMed: 28744319]
6. Buck AK, Serfling SE, Lindner T, Hanscheid H, Schirbel A, Hahner S, et al. CXCR4-targeted theranostics in oncology. Eur J Nucl Med Mol Imaging 2022; 49(12):4133–44. [PubMed: 35674738]
7. Habringer S, Lapa C, Herhaus P, Schottelius M, Istvanffy R, Steiger K, et al. Dual Targeting of Acute Leukemia and Supporting Niche by CXCR4-Directed Theranostics. Theranostics 2018; 8(2):369–83. [PubMed: 29290814]
8. Fletcher EV, Love-Homan L, Sobhakumari A, Feddersen CR, Koch AT, Goel A, et al. EGFR inhibition induces proinflammatory cytokines via NOX4 in HNSCC. Mol Cancer Res 2013; 11(12):1574–84. [PubMed: 24048704]
9. Buck AK, Haug A, Dreher N, Lambertini A, Higuchi T, Lapa C, et al. Imaging of C-X-C Motif Chemokine Receptor 4 Expression in 690 Patients with Solid or Hematologic Neoplasms Using (68) Ga-Pentixafor PET. J Nucl Med 2022; 63(11):1687–92. [PubMed: 35241482]
10. Fischer T, Nagel F, Jacobs S, Stumm R, Schulz S. Reassessment of CXCR4 chemokine receptor expression in human normal and neoplastic tissues using the novel rabbit monoclonal antibody UMB-2. PloS one 2008; 3(12):e4069. [PubMed: 19116653]
11. Mirski SE, Gerlach JH, Cole SP. Multidrug resistance in a human small cell lung cancer cell line selected in adriamycin. Cancer Res 1987; 47(10):2594–8. [PubMed: 2436751]
12. Rodman SN, Spence JM, Ronnfeldt TJ, Zhu Y, Solst SR, O'Neill RA, et al. Enhancement of Radiation Response in Breast Cancer Stem Cells by Inhibition of Thioredoxin- and Glutathione-Dependent Metabolism. Radiat Res 2016; 186(4):385–95. [PubMed: 27643875]
13. Wang H, Bouzakoura S, de Mey S, Jiang H, Law K, Dufait I, et al. Auranofin radiosensitizes tumor cells through targeting thioredoxin reductase and resulting overproduction of reactive oxygen species. Oncotarget 2017; 8(22):35728–42. [PubMed: 28415723]

14. Lapa C, Luckerath K, Rudelius M, Schmid JS, Schoene A, Schirbel A, et al. [68Ga]Pentixafor-PET/CT for imaging of chemokine receptor 4 expression in small cell lung cancer–initial experience. Oncotarget 2016; 7(8):9288–95. [PubMed: 26843617]
15. Ullman-Cullere MH, Foltz CJ. Body condition scoring: a rapid and accurate method for assessing health status in mice. Lab Anim Sci 1999; 49(3):319–23. [PubMed: 10403450]
16. Singh P, Mohammad KS, Pelus LM. CXCR4 expression in the bone marrow microenvironment is required for hematopoietic stem and progenitor cell maintenance and early hematopoietic regeneration after myeloablation. Stem Cells 2020; 38(7):849–59. [PubMed: 32159901]
17. Rosu-Myles M, Khandaker M, Wu DM, Keeney M, Foley SR, Howson-Jan K, et al. Characterization of chemokine receptors expressed in primitive blood cells during human hematopoietic ontogeny. Stem Cells 2000; 18(5):374–81. [PubMed: 11007922]
18. Schottelius M, Ludescher M, Richter F, Kapp TG, Kessler H, Wester HJ. Validation of [(125)I]CPCR4.3 as an investigative tool for the sensitive and specific detection of hCXCR4 and mCXCR4 expression in vitro and in vivo. EJNMMI Res 2019; 9(1):75. [PubMed: 31410585]
19. Pelosi G, Sonzogni A, Harari S, Albini A, Bresaola E, Marchio C, et al. Classification of pulmonary neuroendocrine tumors: new insights. Transl Lung Cancer Res 2017; 6(5):513–29. [PubMed: 29114468]
20. Quinn AM, Chaturvedi A, Nonaka D. High-grade Neuroendocrine Carcinoma of the Lung With Carcinoid Morphology: A Study of 12 Cases. Am J Surg Pathol 2017; 41(2):263–70. [PubMed: 27879513]
21. Rekhtman N, Desmeules P, Litvak AM, Pietanza MC, Santos-Zabala ML, Ni A, et al. Stage IV lung carcinoids: spectrum and evolution of proliferation rate, focusing on variants with elevated proliferation indices. Mod Pathol 2019; 32(8):1106–22. [PubMed: 30923345]
22. Zhang J, Kulkarni HR, Singh A, Niepsch K, Muller D, Baum RP. Peptide Receptor Radionuclide Therapy in Grade 3 Neuroendocrine Neoplasms: Safety and Survival Analysis in 69 Patients. J Nucl Med 2019; 60(3):377–85. [PubMed: 30115686]
23. Uprety D, Halfdanarson TR, Molina JR, Leventakos K. Pulmonary Neuroendocrine Tumors: Adjuvant and Systemic Treatments. Curr Treat Options Oncol 2020; 21(11):86. [PubMed: 32862320]
24. Kalemkerian GP, Akerley W, Bogner P, Borghaei H, Chow LQ, Downey RJ, et al. Small cell lung cancer. J Natl Compr Canc Netw 2013; 11(1):78–98. [PubMed: 23307984]
25. Korde R, Veluswamy R, Barnes G. Small cell lung cancer patients treated with immune checkpoint inhibitor: a systematic literature review of treatment efficacy, safety, and quality of life. Curr Med Res Opin 2022:1–13.
26. Kawaguchi N, Zhang TT, Nakanishi T. Involvement of CXCR4 in Normal and Abnormal Development. Cells 2019; 8(2).
27. Lin Y, Ma Q, Li L, Wang H. The CXCL12-CXCR4 axis promotes migration, invasiveness, and EMT in human papillary thyroid carcinoma B-CPAP cells via NF-kappaB signaling. Biochem Cell Biol 2018; 96(5):619–26. [PubMed: 29316404]
28. Meng W, Xue S, Chen Y. The role of CXCL12 in tumor microenvironment. Gene 2018; 641:105–10. [PubMed: 29017963]
29. Burger M, Glodek A, Hartmann T, Schmitt-Graff A, Silberstein LE, Fujii N, et al. Functional expression of CXCR4 (CD184) on small-cell lung cancer cells mediates migration, integrin activation, and adhesion to stromal cells. Oncogene 2003; 22(50):8093–101. [PubMed: 14603250]
30. Shi Y, Riese DJ, 2nd, Shen J. The Role of the CXCL12/CXCR4/CXCR7 Chemokine Axis in Cancer. Front Pharmacol 2020; 11:574667. [PubMed: 33363463]
31. Kaemmerer D, Reimann C, Specht E, Wirtz RM, Sayeg M, Baum RP, et al. Differential expression and prognostic value of the chemokine receptor CXCR4 in bronchopulmonary neuroendocrine neoplasms. Oncotarget 2015; 6(5):3346–58. [PubMed: 25671300]
32. Crees ZD, Stockerl-Goldstein K, Vainstein A, Chen H, DiPersio JF. GENESIS: Phase III trial evaluating BL-8040 + G-CSF to mobilize hematopoietic cells for autologous transplant in myeloma. Future Oncol 2019; 15(31):3555–63. [PubMed: 31495201]
33. Andtbacka RHI, Wang Y, Pierce RH, Campbell JS, Yushak M, Milhem M, et al. Mavorixafor, an Orally Bioavailable CXCR4 updates Antagonist, Increases Immune Cell Infiltration and

Inflammatory Status of Tumor Microenvironment in Patients with Melanoma. Cancer Res Comm 2022; 2(8):904–13.

34. Salgia R, Stille JR, Weaver RW, McCleod M, Hamid O, Polzer J, et al. A randomized phase II study of LY2510924 and carboplatin/etoposide versus carboplatin/etoposide in extensive-disease small cell lung cancer. Lung Cancer 2017; 105:7–13. [PubMed: 28236984]
35. Knapp FF, Mirzadeh S, Beets AL, Du M. Production of therapeutic radioisotopes in the ORNL High Flux Isotope Reactor (HFIR) for applications in nuclear medicine, oncologyand interventional cardiology. J Radioanal Nucl Ch 2005; 263(2):503–9.
36. Wilson GC, Freeman CM, Kuethe JW, Quillin RC 3rd, Nojima H, Schuster R, et al. CXC chemokine receptor-4 signaling limits hepatocyte proliferation after hepatic ischemia-reperfusion in mice. Am J Physiol Gastrointest Liver Physiol 2015; 308(8):G702–9. [PubMed: 25721302]
37. A genome-wide transcriptomic analysis of protein-coding genes in human blood cells [Internet] 2019 [cited Dec 20]. Available from: https://www.proteinatlas.org/ENSG00000121966-CXCR4/single+cell+type.
38. Friesecke I, Beyrer K, Fliedner TM, system MtMtpfravaabfacg. How to cope with radiation accidents: the medical management. Br J Radiol 2001; 74(878):121–2. [PubMed: 11718381]
39. Sun J, Ramos A, Chapman B, Johnnidis JB, Le L, Ho YJ, et al. Clonal dynamics of native haematopoiesis. Nature 2014; 514(7522): 322–7. [PubMed: 25296256]
40. Busch K, Klapproth K, Barile M, Flossdorf M, Holland-Letz T, Schlenner SM, et al. Fundamental properties of unperturbed haematopoiesis from stem cells in vivo. Nature 2015; 518(7540): 542–6. [PubMed: 25686605]
41. Park EA, Graves SA, Menda Y. The Impact of Radiopharmaceutical Therapy on Renal Function. Semin Nucl Med 2022; 52(4): 467–74. [PubMed: 35314056]
42. Shibuta K, Mori M, Shimoda K, Inoue H, Mitra P, Barnard GF. Regional expression of CXCL12/CXCR4 in liver and hepatocellular carcinoma and cell-cycle variation during in vitro differentiation. Jpn J Cancer Res 2002; 93(7):789–97. [PubMed: 12149145]

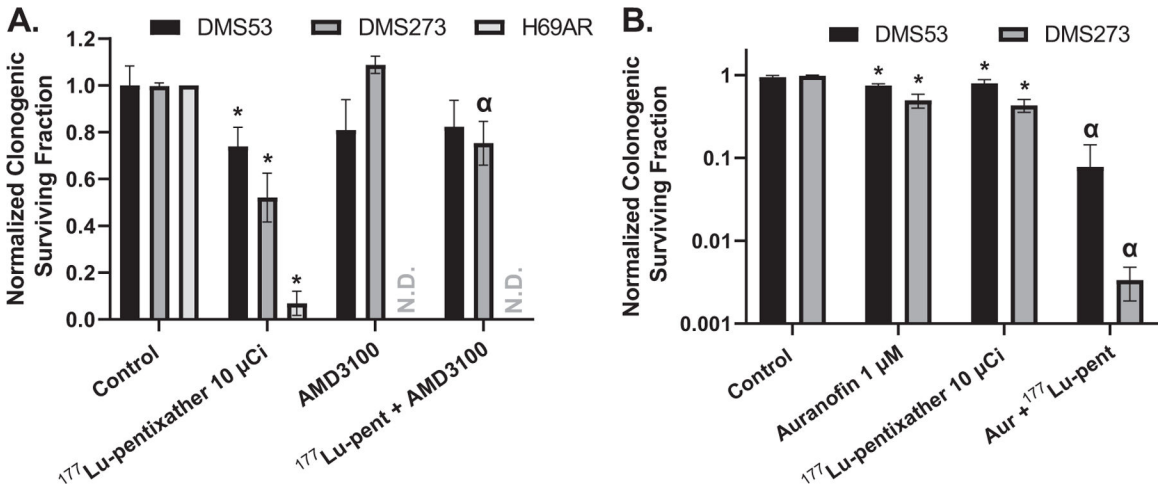

FIG. 1.

Treatment with ^{177}Lu-pentixather causes clonogenic cell death in a CXCR4 specific mode and auranofin enhances the toxicity in a SCLC. Panel A: Exponentially growing DMS53, DMS273 and H69AR cells were treated with 30 μM AMD3100 starting 5 min before and during the addition of 10 μCi ^{177}Lu-pentixather for 3 h followed by assessment of clonogenic survival. N = 2–4 independent experiments; Panel B: Exponentially growing DMS53 and DMS273 were treated with 10 μCi ^{177}Lu-pentixather and/or 1 μM auranofin for 3 h followed by assessment of clonogenic survival. N = 3 independent experiments. Colony counts were normalized to respective cell lines without treatment. *Significantly different than control, ά significantly different than either drug alone. ND = not determined.

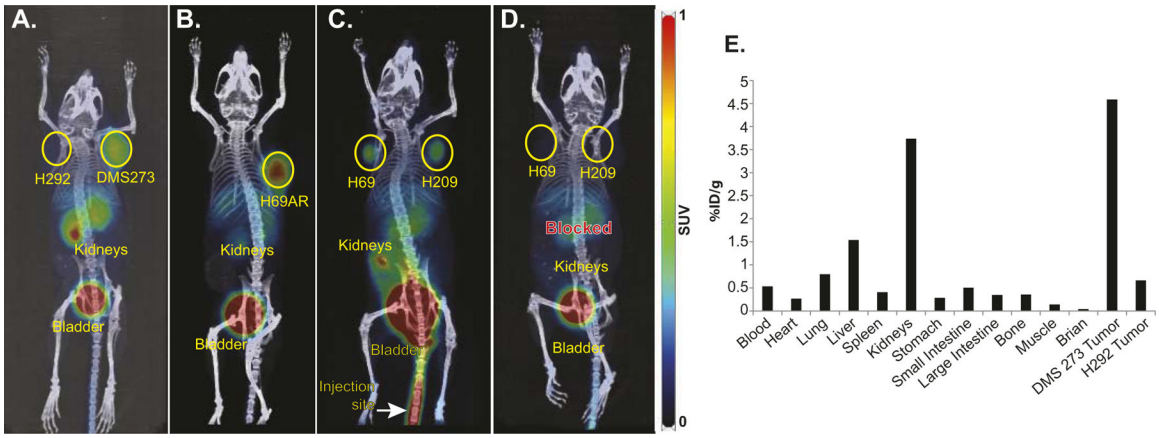

FIG. 2.

PET/CT imaging using ^{68}Ga-pentixafor demonstrates specific targeting of CXCR4 in SCLC. The mice showed the expected biodistribution with radiotracer uptake seen in CXCR4-expressing tumors as well as excretion via the kidneys and bladder. In Panels A–D, images of mice bearing SCLC xenografts were taken 1 h after injection with 168–334 μCi ^{68}Ga-pentixafor. PET images were set with a scale of 0–1. Panel A: H292 NSCLC xenograft was used as a negative control and DMS273 SCLC xenograft; Panel B: H69AR SCLC xenograft; Panel C: H69 and H209 SCLC; Panel D: Same mouse as Panel C with 50 μg AMD3100 (unlabeled CXCR4 antagonist) co-injected with ^{68}Ga-pentixafor; Panel E: Bio-distribution of ^{68}Ga-pentixafor in mouse shown in Panel A, measured ~1 h 45 min after injection.

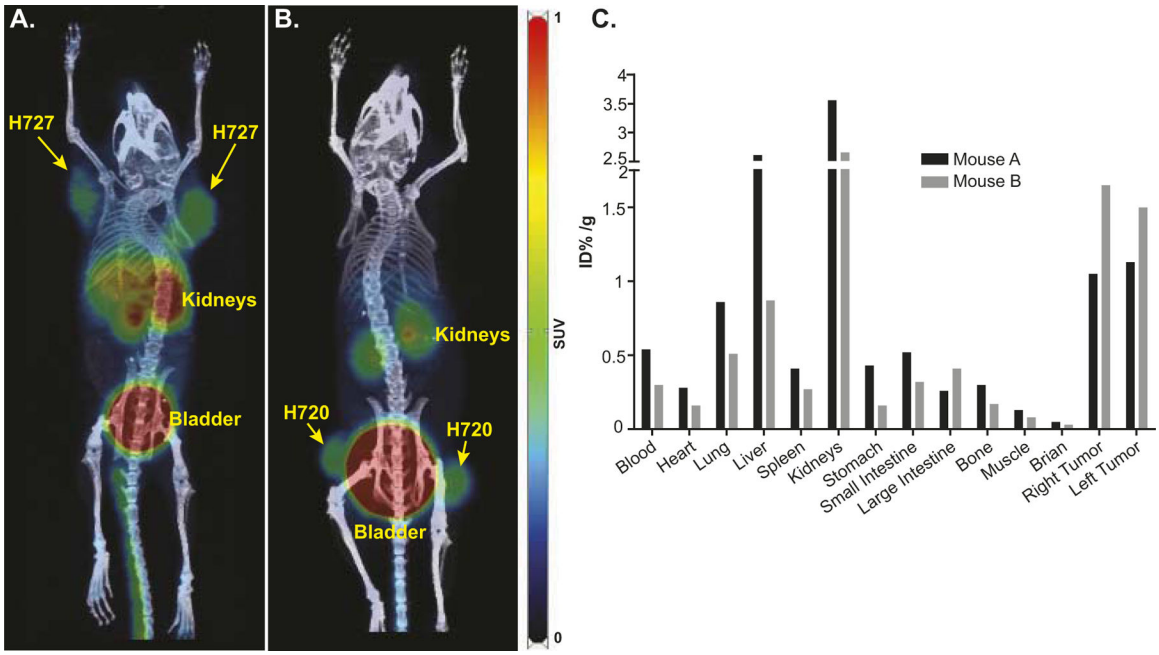

FIG. 3.

PET/CT imaging using ^{68}Ga-pentixafor demonstrates specific targeting of CXCR4 in lung NECs. The mice showed the expected biodistribution with radiotracer uptake seen in CXCR4-expressing tumors as well as excretion via the kidneys and bladder. Images of mice bearing lung NEC xenografts were taken 2 h after injection with 288 and 307 μCi ^{68}Ga-pentixafor, respectively. Panel A: H727 epithelial lung carcinoid xenograft; Panel B: H720 atypical lung carcinoid xenograft. PET images were set with a scale as 0–1; Panel C: Bio-distribution of ^{68}Ga-pentixafor was measured ~1 h 45 min after injection.

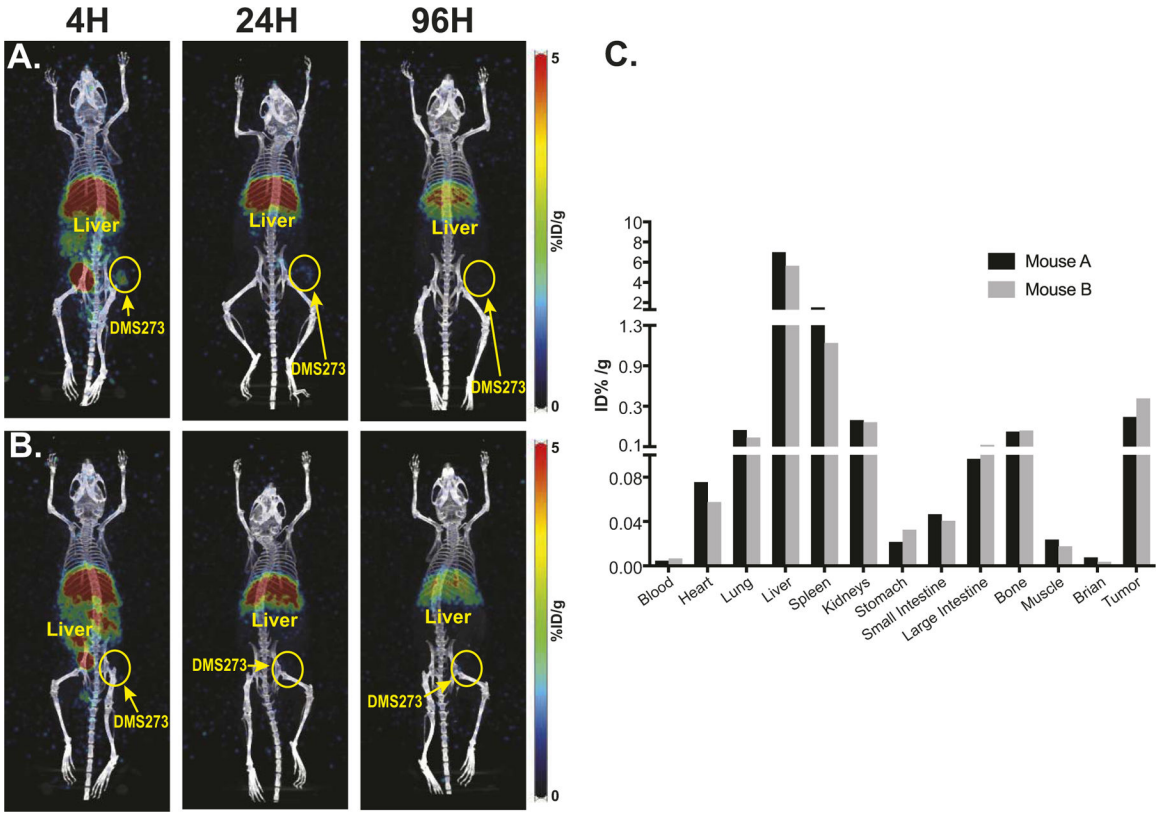

FIG. 4.

Sequential SPECT imaging and bio-distribution indicates liver and spleen are the major sites of tracer distribution. Panel A: Mouse bearing DMS273 xenograft on the hind flank was injected iv with 425.9 μCi of ^{177}Lu-pentixather. Panel B: A second mouse bearing a smaller DMS273 xenograft on the hind flank was injected iv with 417.7 μCi of ^{177}Lu-pentixather; Panel C: Quantification of radiotracer 100 h after ^{177}Lu-pentixather injection.

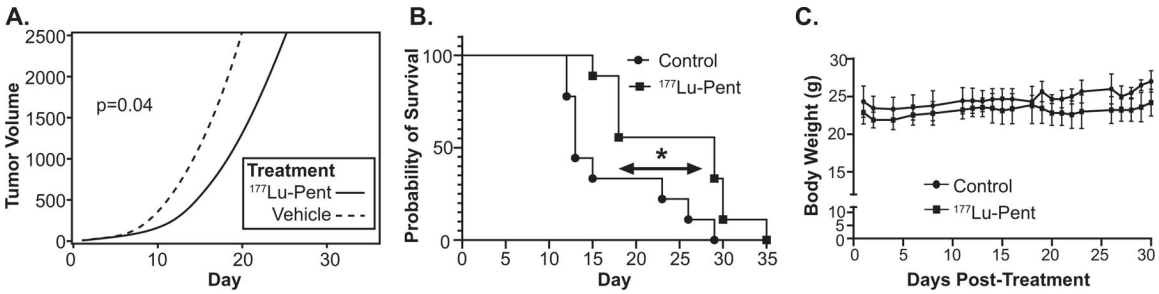

FIG. 5.

Treating mice bearing SCLC xenografts with ^{177}Lu-pentixather significantly decreases growth rate and prolongs survival without causing weight loss. Nude mice were injected with 1 million DMS273 SCLC cells in flanks and allowed to grow for 7 days followed by a tail vein injection of 25 μCi/g body weight ^{177}Lu-pentixather on day 1. Panel A: Tumor sizes were measured using calipers throughout the experiment and tumor volume calculated, resulting in repeated measurements for each mouse. Non-linear mixed effects regression models used to estimate tumor growth curves showed a significant (P = 0.04) delay in tumor growth rate in treated mice vs. control mice; Panel B: When tumors measured 15 mm in diameter, mice were euthanized, and the Kaplan-Meier plot was used to estimate the survival curves. Log-rank (Mantel-Cox) test resulted in a significantly (P = 0.012) longer survival in treated mice vs control mice; Panel C: There were no significant weight differences between treated and non-treated mice.

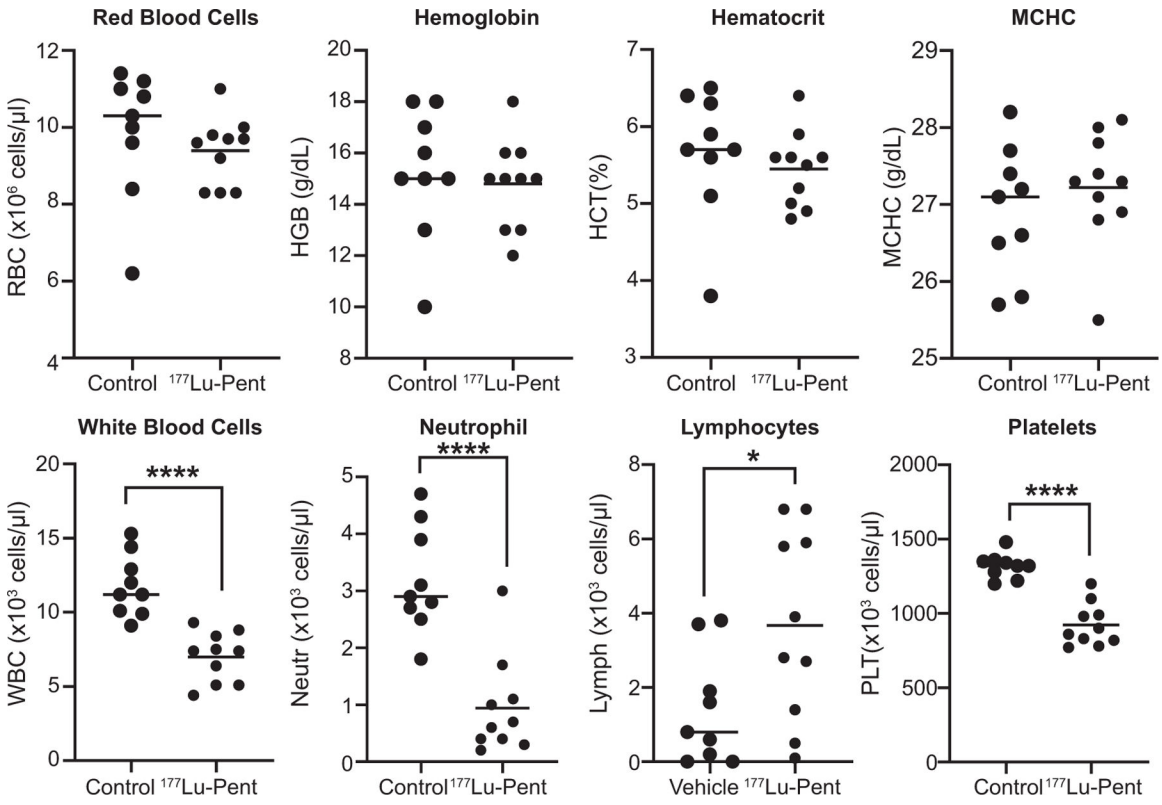

FIG. 6.

Complete blood count performed 13 days after ^{177}Lu-pentixather injection demonstrates decrease in white blood cells and platelets. Blood was taken from the mandibular vein of mice as described in Fig. 4 and CBC was performed. Unpaired T test resulted in significant differences (****P < 0.001) between treated and non-treated mice and a significant (*P = 0.05) increase in lymphocytes.

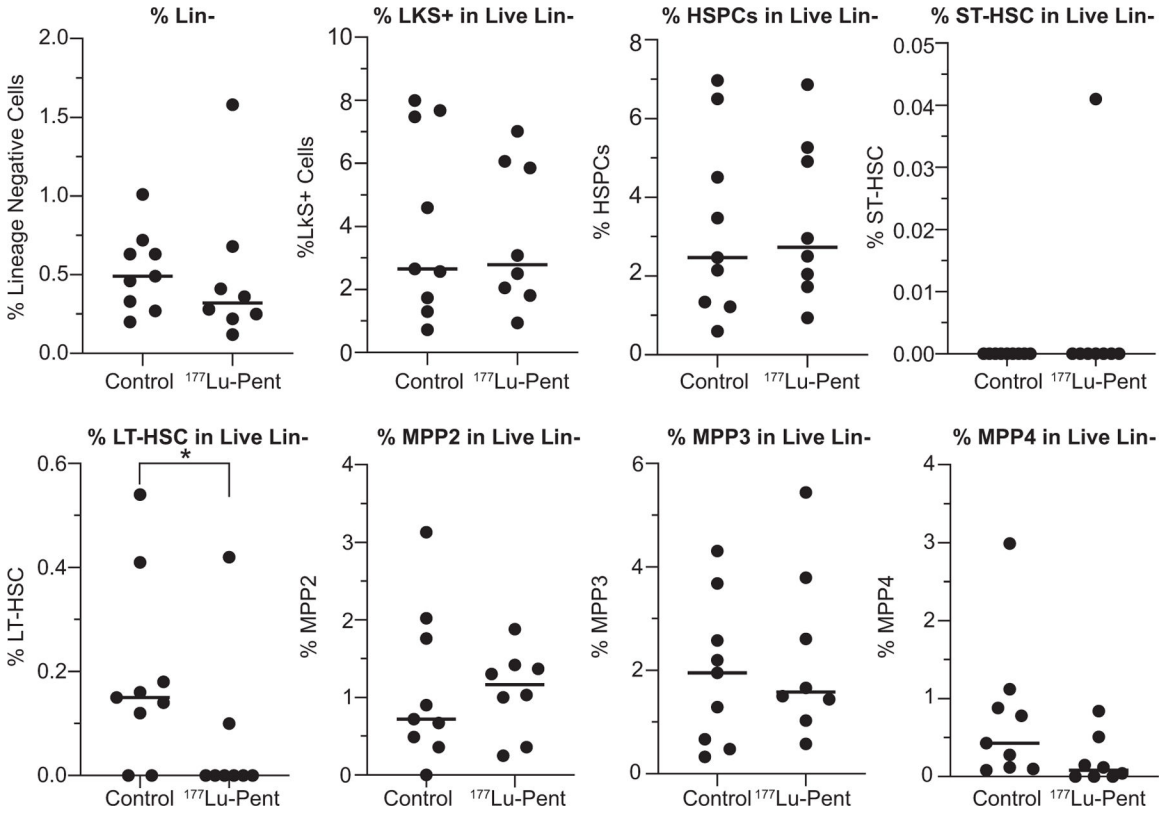

FIG. 7.

Analysis of bone marrow cells demonstrates a significant decrease in %LT-HSC live Lin- cells in mice treated with 25 μCi/g Lu-pentixather. When tumors reached criteria for euthanasia, mice femur bone marrow cells were harvested, stained, and analyzed by flow cytometry. HSPC: hematopoietic and progenitor stem cell; ST-HSC: short-term hematopoietic stem cell; LT-HSC: long-term hematopoietic stem cell; MPP2; MPP3: myeloid-biased MPP subsets; MPP4: lymphoid-primed progenitors.

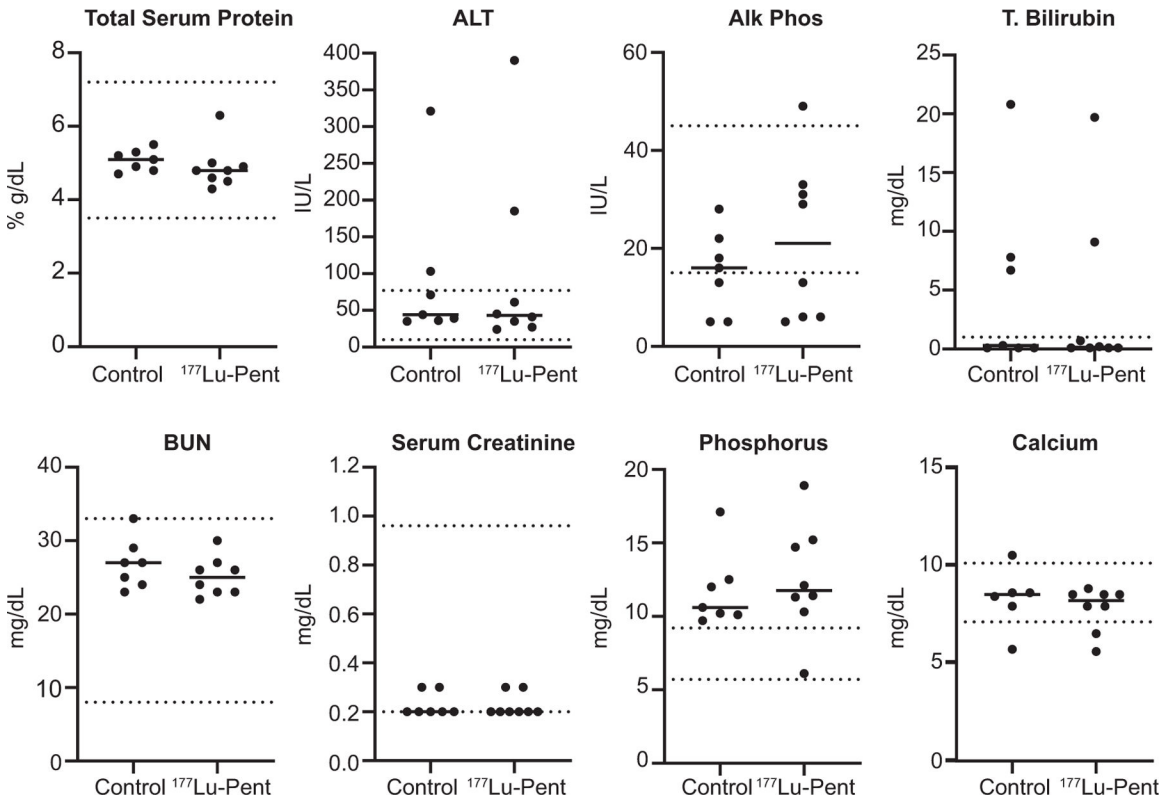

FIG. 8.

Serum clinical chemistry demonstrated no differences between treated and control mice. Serum was taken via cardiac puncture on the day of euthanasia from mice and clinical chemistry performed. Unpaired T test resulted in no significant differences between treated and non-treated mice.

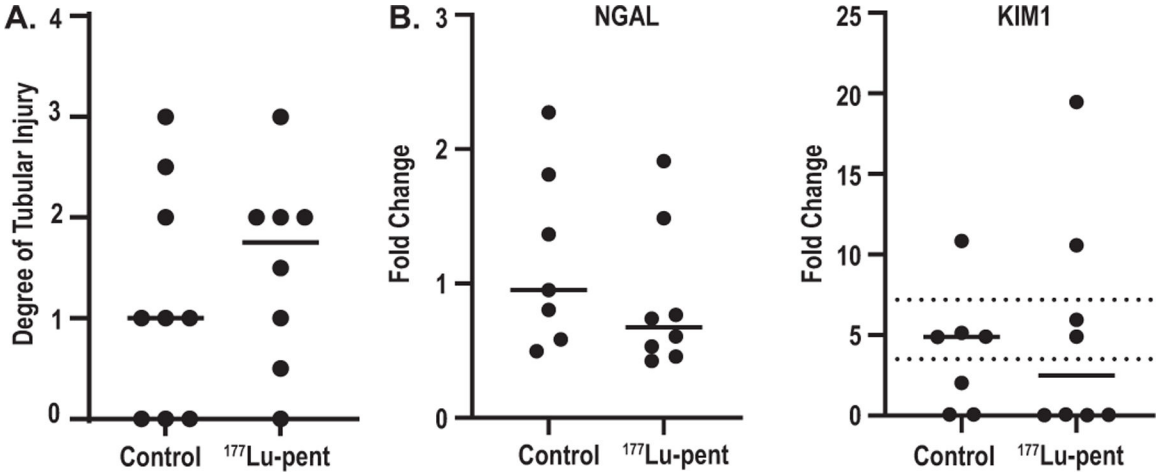

FIG. 9.

There was no significant damage to the kidneys as demonstrated via pathological examination or biomarkers of damage. After euthanasia mouse kidneys were stained with H&E, PAS, and Masson's Trichrome and examined by a blinded pathologist for tubuloninterstitial inflammation, interstitial fibrosis, and glomerular changes (none were noted). Panel A: Tubular injury was assessed via stained bodies of various sizes, vacuolization, loss of epithelial cells nuclei, dark acidophilic cytoplasm, loss of tubular epithelial cells into tubular lumen, and acellular sections of tubules (scoring: 0 = absent, 1 = mild (1–10%) 2 = moderate (11–25%) 3 = severe (26–50%) 4 = very severe > 50% glomeruli with any degree of sclerosis or collapse and thrombo-necrotic lesions). There were no significant differences between treatment and control groups; Panel B: Quantitative PCR on mRNA isolated from mouse kidneys was performed using primers for NGAL and KIM1.

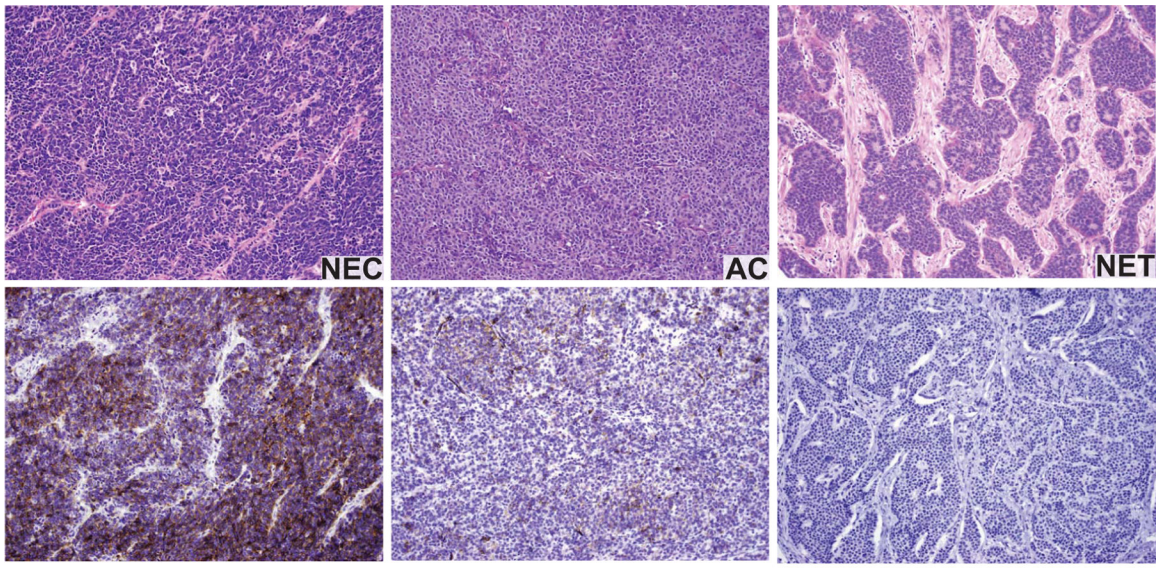

CXCR4 Expression (Mean H-score, if positive)		
Tumor Type and Site (n)	**Any Positivity**	**H-score >30**
All NEC (n=95)	84% (120)	67% (148)
Lung (31)	93.5% (150)	77% (179)
Skin (43)	81% (91)	58% (124)
Extrapulmonary visceral (21)	76% (131)	71% (139)

FIG. 10.

CXCR4 is expressed on human pulmonary NECs and NETs. Representative immuno-histochemical staining of CXCR4 using CXCR4 antibody (clone UMB-2) on human tissue microarrays of 95 poorly differentiated NECs.

TABLE 1

Human Lung Carcinoid and Small Cell Lung Cancer Cell Lines Express CXCR4

Cell type	Cell line	Fold change	MFI
Mucoepidermoid lung carcinoma (negative control)	H292	1 ± 0.2	1 ± 0.08
SCLC	DMS53	2 ± 0.4	4.8 ± 0.6
Typical lung carcinoid	H727	28 ± 6.6	4.3 ± 0.4
Atypical lung carcinoid	H720	203 ± 57.3	N.D.
SCLC	H446	141 ± 21.8	N.D.
SCLC	H209	280 ± 94.8	10.3 ± 2.3
SCLC	H69	142 ± 17.3	86.3 ± 6.3
SCLC	DMS273	299 ± 63.0	44.5 ± 5.9
SCLC (multi-drug resistant)	H69AR	356 ± 87.5	84.9 ± 24.2

Notes. CXCR4 levels were quantified using qPCR or median fluorescent intensity (MFI) via flow cytometry using anti CXCR4 antibody as described in method. A minimum of 3 experiments used for each analysis. N.D.= not determined

TABLE 2

CXCR4 is Expressed on Most Lung NECs and Atypical Carcinoids

Tumor type (n)	Any positivity	H-score >30
Lung NECs (n = 21)	100%	76% (181)
Typical carcinoid (n = 5)	40%	0%
Atypical carcinoid (n = 10)	80%	60% (143)

Notes. Expression of CXCR 4 was measured prospectively on a cohort of lung NET/NEC at the University of Iowa. Mean H-score, if positive.